nature geoscience

Article

https://doi.org/10.1038/s41561-022-01105-y

Reduced phosphorus availability in paddy soils under atmospheric CO_2 enrichment

Received: 10 June 2022

Accepted: 22 November 2022

Published online: 19 January 2023

Check for updates

Yu Wang[1,18], Yuanyuan Huang[2,18], Lian Song[1], Jiahui Yuan[1], Wei Li[3], Yongguan Zhu[4,5], Scott X. Chang[6], Yiqi Luo[7], Philippe Ciais[8], Josep Peñuelas[9,10], Julie Wolf[11], Barbara J. Cade-Menun[12], Shuijin Hu[13], Lei Wang[14], Dengjun Wang[15], Zengwei Yuan[16], Yujun Wang[1], Jishuang Zhang[1,17], Ye Tao[1], Shenqiang Wang[1], Gang Liu[1], Xiaoyuan Yan[1] & Chunwu Zhu[1] ✉

Phosphorus is an essential element for plant metabolism and growth, but its future supply under elevated levels of atmospheric CO_2 remains uncertain. Here we present measurements of phosphorus concentration from two long-term (15 and 9 years) rice free air carbon dioxide enrichment experiments. Although no changes were observed in the initial year of the experiments, by the end of the experiments soil available phosphorus had declined by more than 20% (26.9% and 21.0% for 15 and 9 years, respectively). We suggest that the reduction can be explained by the production of soil organic phosphorus that is not in a readily plant-available form, as well as by increased removal through crop harvest. Our findings further suggest that increased transfers of plant available phosphorus from biological, biochemical and chemical phosphorus under anthropogenic changes are insufficient to compensate for reductions to plant available phosphorus under long-term exposure to elevated CO_2. We estimate that reductions to rice yields could be particularly acute in low-income countries under future CO_2 scenarios without the input of additional phosphorus fertilizers to compensate, despite the potentially reduced global risk for phosphorus pollution.

A higher atmospheric carbon dioxide (CO_2) concentration generally stimulates the photosynthesis of C3 species, a response widely known as the CO_2 fertilization effect[1]. Yields of C3 crops have been found to increase by 18%, on average, under elevated CO_2 (eCO_2) across multiple free air CO_2 enrichment (FACE) experiments[2]. The CO_2 fertilization effect has long been viewed as a 'silver lining' with respect to the threats to global food security arising from climate change. Global food security is currently facing unprecedented challenges from the recent (2022) Russo–Ukrainian War and worldwide record-breaking occurrences of climate extremes. However, nutrient limitation inhibits this CO_2 fertilization effect[3–5]. Nitrogen (N) and phosphorus (P) are essential nutrients that are required for multiple biochemical processes such as plant photosynthesis, growth and physiology. The constraint of N availability on the positive response of biomass production (or yields) under eCO_2 has been documented in a number of FACE experiments, revealing complex interactions of eCO_2 with photosynthetic enzymes, plant N use strategies and soil N supply that can shift the magnitude, timing and dominant mechanism of the eCO_2 response[2,3,6–8]. For example, Reich and Hobbie[8] reported diminishing eCO_2 effects in enhancing plant biomass production due to declining soil N availability, a response detected in long-term (~10 years), but not short-term (<3 years) FACE experiments. Low P supply from soils limits leaf P content and reduces the P-containing molecules (for example, adenosine triphosphate, sugar phosphates, phospholipids, nucleotides and nucleic acids) that

A full list of affiliations appears at the end of the paper. ✉e-mail: cwzhu@issas.ac.cn

are critical in leaf photosynthesis and plant growth[9,10]. Compared to N, there are fewer studies of the interaction of P availability and eCO_2, especially from long-term field experiments.

The small number of existing studies found both increases and decreases of P availability in response to eCO_2 (Supplementary Table 1). These differences reflect a critical knowledge gap in eCO_2-induced plant P demand, P acquisition strategies, soil microbial activities and geochemical processes that alter soil P dynamics[11] across agroecosystems and time. eCO_2 enhanced the demand for P by leaf photosynthesis and plant growth (that is, rice tiller number and spikelet density)[6], but also the supply of P through stimulated root exudates to mine P[12], altered microbial activities[13], accelerated decomposition soil organic matter and shifted allocation of soil P among different fractions. However, the net response and long-term trajectory of soil P availability remains largely unknown. This gap is of crucial relevance to food security and environmental P pollution in the future.

Soil P is unevenly distributed across regions and ecosystems[14,15]. Historical excessive P fertilization to maximize crop production has led to the accumulation of soil P in some regions, such as Europe, North America and southeastern Asia[16]. Accumulated soil P is susceptible to loss to water bodies through surface and subsurface runoff, leaching and erosion, which contribute to eutrophication[16,17]. In contrast, in regions without increased P fertilizers supply, or with highly weathered soils that strongly bind the added P fertilizer, prolonged P deficit could limit yields, which may be exacerbated under future continuously increasing levels of eCO_2 and global changes[18,19].

Rice is the primary food staple for more than 50% of the world's population and provides more than 20% of global human caloric intake. Paddy fields, where most rice is grown, constitute the largest man-made wetlands on Earth[20], accounting for >12% of global cropland area, and the total acreage is increasing rapidly, especially in Africa[21]. Because of their frequent irrigation–drainage cycles, rice paddy fields are at particularly high risk of P loss through surface runoff. Accordingly, rice paddy fields are one of the largest sources of P contributing to agricultural pollution in China[22]. Notwithstanding the pollution risk associated with current rice cropping, the expected eCO_2 enhancement of rice production is conditioned upon additional nutrient supply, which will be challenging for regions that are already suffering from P limitation. eCO_2 can potentially alter plant P uptake[23,24], soil microbial processes[12,13] or soil P supply[25,26], which may accelerate, eliminate or delay the impact of P limitation or pollution in different regions. Among a small number of eCO_2 experiments focusing on P dynamics, most are short-term (<3 years) and conducted under laboratory or greenhouse conditions for upland crops[25–27], leaving the long-term effect of eCO_2 on the transformation and availability of soil P in paddy fields largely underexplored.

We hypothesize that the increase in P consumption driven by plant demand under eCO_2 outpaces the increase of P sources to plants by recycling and mobilization. We use two unique long-term rice FACE experiments established in China (Supplementary Fig. 1) to test this hypothesis and understand the implications of altered soil P dynamics for rice production and environmental P pollution. The two study sites, $P_{L\text{-}M}$ and P_H, have a low-to-moderate (5–20 mg kg^{-1}) and high (>20 mg kg^{-1}) concentrations of Olsen P (available P extracted by $NaHCO_3$, pH 8.5), respectively (Methods).

Changes in soil P pools in response to eCO_2

Both experiments showed decreased soil available P but increased soil organic P after several years of eCO_2 treatments (Fig. 1a, Table 1 and Extended Data Figs. 1 and 2a–d). Here, soil available P refers to labile inorganic P (P_i) for microbial and vegetation uptake in the short term (resin–P and $NaHCO_3$–P_i), and organic P (P_o, the sum of $NaHCO_3$–P_o and NaOH–P_o) includes the extracted available organic fractions[28] (Methods). In study $P_{L\text{-}M}$, soil available P was higher under elevated (eCO_2) than ambient (aCO_2) treatments in year 1, but soil available P decreased by 15.6%, 29.3% and 21.4% in years 6, 12 and 15, respectively. Soil organic P (P_o) increased by 24.1% and 22.0% in years 12 and 15, respectively. Secondary mineral P (NaOH–P_i, corresponding to iron and aluminium phosphates) showed no big changes under eCO_2. Occluded P (residual P, which has been suggested to be occluded by soil minerals[28]) was lower under eCO_2 only in year 1. Soil primary mineral P (HCl–P, associated with poorly soluble calcium phosphates) decreased from year 12, which was further verified by the results of solid-state ^{31}P NMR spectroscopy (Extended Data Fig. 2a,b). We found a significant impact of year × CO_2 interactions ($P = 0.021$; Table 1), from an initial enhancement to the later reductions by eCO_2, that were statistically significant in years 12 ($P = 0.019$) and 15 ($P = 0.047$; Table 1). Primary mineral P, secondary mineral P and P_o showed significant ($P < 0.05$) changes through time, although the effect of eCO_2 was not statistically significant ($P > 0.05$; Supplementary Table 2). In study P_H, after nine years of exposure to eCO_2, soil available P decreased (Fig. 1a and Table 1) by 28.3%, from 123.6 (aCO_2) to 88.6 mg kg^{-1} (eCO_2), and P_o increased by 9.08%, from 43.5 (aCO_2) to 47.5 mg kg^{-1} (eCO_2).

The results held when we grouped resin–P, $NaHCO_3$–P_i and $NaHCO_3$–P_o as available P to account for the indirect uptake of organic P by plants, and soil organic P refers to NaOH–P_o. We also found a decrease in available P under eCO_2 when we used the sum of soil available P (resin–P and $NaHCO_3$–P_i) plus secondary mineral P to indicate available P in a timescale that is relevant to crop growth (up to months)[17,29] to account for P transfers among inorganic pools. When we used Olsen P to quantify available P, we reached the same conclusion on the reduction of available P under eCO_2 (Supplementary Fig. 2). In addition, we further confirmed a reduction of soil available P and an increase in soil organic P through liquid-state ^{31}P NMR (Extended Data Fig. 2c,d), with inorganic P corresponding to orthophosphate and pyrophosphate, and organic P including the sum of phosphate monoesters and diester (mainly DNA–P).

Attribution of the changes in response to eCO_2

The increase of P in soil forms not directly plant-available, as soil organic P or in crop biomass caused the reduction of available P under long-term eCO_2, despite the acceleration of P transfers into available P in our rice paddy fields. The CO_2 fertilization effect most likely caused a positive effect on rice growth[30]. Rice grain yields increased from 7.40 ± 0.14 (aCO_2) to 8.32 ± 0.23 (eCO_2) Mg ha^{-1} in study $P_{L\text{-}M}$ and 8.51 ± 0.05 (aCO_2) to 9.39 ± 0.16 (eCO_2) Mg ha^{-1} in study P_H (Extended Data Fig. 3). In study $P_{L\text{-}M}$, P concentrations in grain and straw were similar between aCO_2 (grain, 2.77 g kg^{-1}; straw, 1.47 g kg^{-1}) and eCO_2 (grain, 2.72 g kg^{-1}; straw, 1.47 g kg^{-1}) at the harvest stage. In study P_H, harvested grain and straw had a higher P concentration under eCO_2 (grain, 2.85 g kg^{-1}; straw, 2.51 g kg^{-1}) than aCO_2 (grain, 2.45 g kg^{-1}; straw, 1.86 g kg^{-1}) at the harvest stage (Extended Data Fig. 3). These results are provided in Extended Data Fig. 4a, and are similar to the conclusions of Ainsworth and Long[2], who reported that eCO_2 caused a significant increase in rice yield, but no significant differences for P content (Extended Data Fig. 4b). As a result, more P was removed from the system through crop harvest (grain + above-ground straw) under eCO_2 (Fig. 1b and Extended Data Fig. 4). Compared to P inputs into the paddy field through fertilizers, eCO_2 resulted in a slightly negative P-balance (fertilizer inputs − harvest outputs; Methods), whereas there was a slightly positive P-balance under aCO_2 in study $P_{L\text{-}M}$. Moreover, eCO_2 led to a stronger negative P-balance than aCO_2 in study P_H (Fig. 1b). Overall, eCO_2 aggravated negative P-balances. Atmospheric P deposition and P runoff or leaching losses[31,32] are similar between aCO_2 and eCO_2.

Meanwhile, multiple lines of evidence indicate the acceleration of below-ground biochemical, microbial, chemical and root activities that could potentially increase transfers of P into available forms. We observed an enlarged rice root scale and enhancement in the morphology of root systems for root acquisition of available P[33,34] under eCO_2 (Extended Data Fig. 5). The eCO_2 increased bacterial biomass[12,13],

https://doi.org/10.1038/s41561-022-01105-y

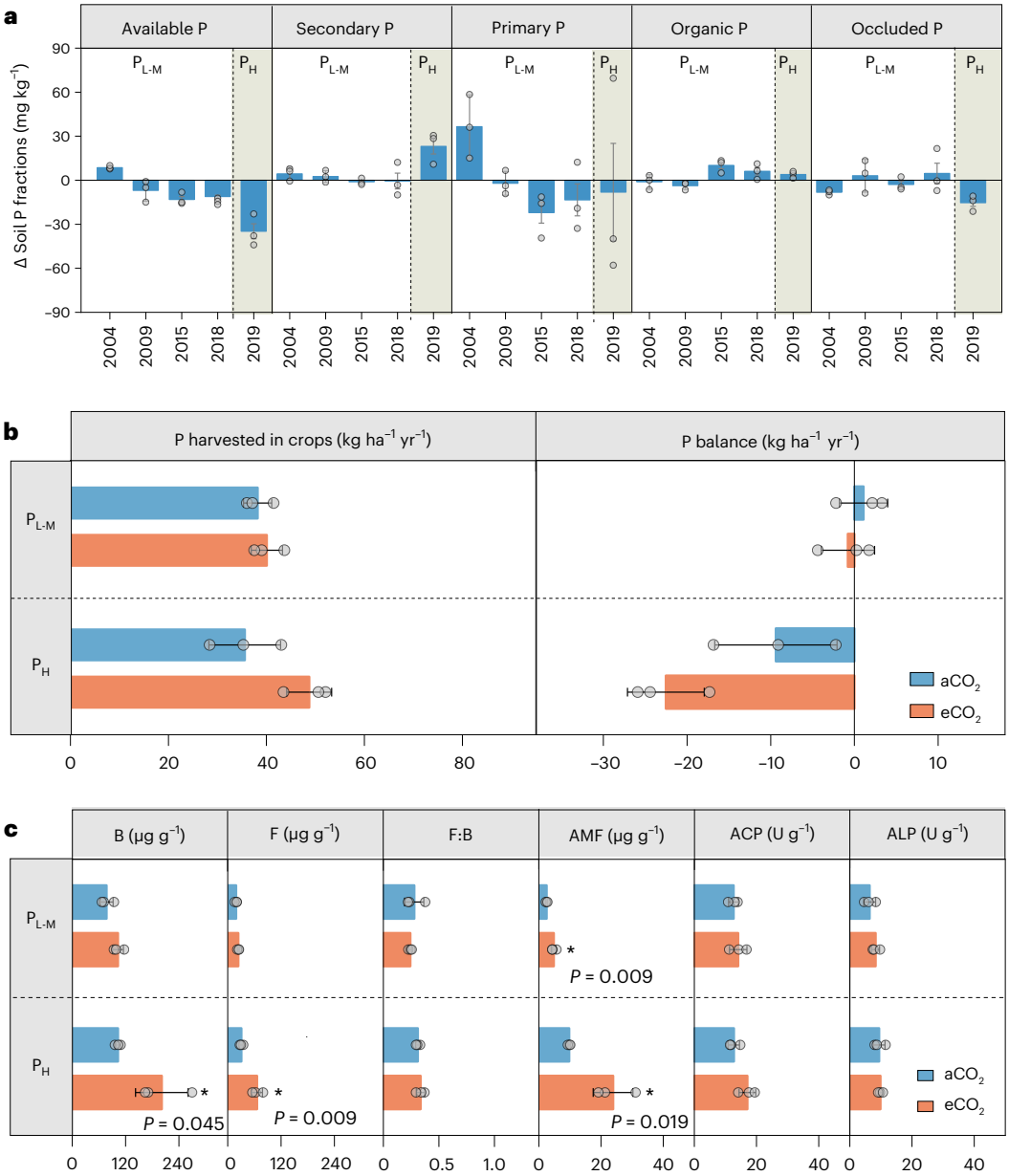

Fig. 1 | Responses of plant and soil to eCO_2 in two rice FACE experiments. **a**, The difference in soil P pool sizes between eCO_2 and aCO_2 ($eCO_2 - aCO_2$): soil available P, resin–P and $NaHCO_3$–P_i; secondary P, NaOH–P_i; primary P, HCl–P_i; organic P, $NaHCO_3$–P_o and NaOH–P_o; occluded P, residual-P. **b**, P-harvest and P-balance (P input through fertilizer − P output through crop harvest). **c**, Soil bacterial biomass (B), fungal biomass (F), F:B ratio, AMF and the activities of ACP and ALP. Data are presented as mean ± s.d. ($n = 3$). The asterisks indicate significant differences between means at $P < 0.05$. Actual values for **a** are provided in Extended Data Fig. 1, and statistical tests are provided in Table 1 and Supplementary Table 2. $P_{L\text{-}M}$ and P_H were initiated in 2004 and 2011, respectively.

total fungal biomass and the biomass of arbuscular mycorrhizal fungi (AMF)[35] in varying degrees in both studies (Fig. 1c). The activities of the enzymes acid phosphatase (ACP) and alkaline phosphatase (ALP) were also higher under eCO_2 compared to aCO_2 (Fig. 1c), suggesting that biological and biochemical mineralization of organic P was probably enhanced by eCO_2. Increased microbial biomass also indicated more microbial P demand and immobilization of P for microbial activities[11]. The correlations between microbial biomass and available P were positive in general except in study P_H under aCO_2 (Extended Data Fig. 6). This positive correlation is stronger under more P-limited conditions (that is, study $P_{L\text{-}M}$ under eCO_2), indicating that the net microbial effect (decomposition and immobilization) acted to increase available P under eCO_2. We also found a reduction in primary mineral P under eCO_2 in both experiments, which may indicate the transfer of mineral P into more available forms, despite large uncertainties for the measurements (Fig. 1a). Primary mineral P contains recalcitrant P that is slow to dissolve in the soil solution and thus is unlikely to be a major contributor to plant available P in the short term. Several other FACE experiments have also shown reductions of recalcitrant P fractions in response to five years or seven years of exposure to eCO_2 and the increased biotic P demand[25,36,37]. The declines in primary P might be due in part to enhanced root growth and organic acid exudation, which can promote the dissolution or desorption of non-labile mineral P[23].

It is likely that the eCO_2-induced enhancement of net P mineralization dominated the initial response in our study $P_{L\text{-}M}$ of increasing available P_i. Hasegawa and colleagues[38] also attributed the increase of phosphate in their *Eucalyptus* woodland FACE experiment to a higher P mineralization rate under eCO_2. In our long-term experiments, this

https://doi.org/10.1038/s41561-022-01105-y

Table 1 | Statistical analysis of variance of CO_2 year and effect on soil available P

Site	Effect		Available P (mg kg^{-1})		
			F	P	Method
$P_{L\text{-}M}$	Overall effect	Year	**17.26**	**0.000**	Analysis of variance with repeated measures
		CO_2	2.300	0.204	
		Year×CO_2	**4.707**	**0.021**	
	CO_2 simple effect	2004	3.041	0.156	
		2009	0.597	0.483	
		2015	**14.39**	**0.019**	
		2018	**8.032**	**0.047**	
P_H	CO_2	2019	**20.39**	**0.011**	Tukey's test

Effects of year and CO_2 on soil available P are shown. Year is included in the statistical model as a continuous variable. Effects of year and CO_2 are shown in Fig. 1 and Extended Data Fig. 1. Significant effects ($P<0.05$) are shown in bold. $P_{L\text{-}M}$ and P_H were initiated in 2004 and 2011, respectively.

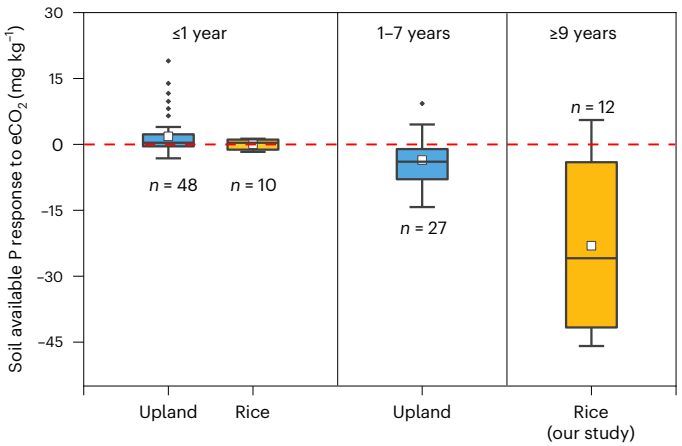

Fig. 2 | Changes of soil available P concentrations under eCO_2 relative to aCO_2 in upland (non-rice) crops and paddy rice. The results are based on data from this study and the literature (Supplementary Table 1). The values indicate the differences in soil P pool sizes between eCO_2 and aCO_2 ($eCO_2 - aCO_2$). The line and open square in each box represent the median and mean, respectively. Whiskers mark the 10th and 90th percentiles, and the outliers are shown as dots. *n* indicates the number of experimental outcomes. Soil available P was determined by different methods, including resin–P, $NaHCO_3$–P_i and Olsen P.

positive contribution to available P was not big enough to compensate for the consumption of available P through biological uptake after the initial year. We did not quantify the biomass inputs (mostly roots) into soils after crop harvest. It is highly likely that inputs of plant organic matter into soils were increased under eCO_2, which is supported by our root imagery and length data (Extended Data Fig. 5). These plant-sourced organic P inputs explained the higher organic P observed in our long-term experiments under eCO_2[11]. The temporal shift in available P response from our study showed a reduction in available P, in which available P was taken up by plants and converted into unavailable forms that reduced available P through time.

Synthesis of the eCO_2 effect on available P

The direction of the response of available P to eCO_2 remains largely elusive across ecosystems and studies, with increased, no change or decreased available P (Table 1, Extended Data Fig. 7 and Supplementary Table 1). In farmlands, we found that the experiment duration was critical in elucidating the divergent responses of available P to eCO_2 (Fig. 2). Generally speaking, the longer the experimental duration (≤1 year, 1–7 years and ≥9 years), the stronger the reduction of available P in response to eCO_2 based on synthesizing results from existing FACE, open-top chambers, and controlled growth chambers experiments. To the best of our knowledge, no previously published studies have conducted decade-long FACE experiments to investigate soil P dynamics in agroecosystems, and long-term experiments on this topic are scarce. Nevertheless, our study is not the only study to find available P reductions under eCO_2 in farmlands. For example, Jin and colleagues[25] found decreases in both available P and organic P after seven years of eCO_2 in upland farms (wheat–pulse rotation), which was linked to crop harvest and microbial mineralization of organic P. These results highlight the fact that the cumulative impacts of long-term eCO_2 on soil P transformations in agroecosystems might not be captured by short-term experiments (see the conceptual model in Fig. 3).

Global risks of yield reduction and potential P pollution

The observed reduction of plant-available P in our long-term rice FACE experiments has important implications for future P management in rice paddy fields. Country-level P balances (input − removal) are negative across all major rice production countries except India under eCO_2 (Supplementary Tables 3 and 4), indicating possible global reductions of P availability for rice production in the future. Currently, ~35% of the global rice paddy area is under an extremely high risk of yield reduction (level 5, Extended Data Fig. 8; see Methods for the definition of risk levels), corresponding to Olsen P < 5 mg kg^{-1} based on known studies[39–41] (Methods), and 15% of the rice paddy fields are classified as potentially problematic for P pollution (Olsen P > 40 mg kg^{-1}, level 1 in Extended Data Fig. 8), with lost P polluting water bodies[39,42,43]. Here, we project that 55% of rice paddy fields will experience increased yield reduction risks due to P deficiency under eCO_2 (200 µmol mol^{-1}) compared to aCO_2 (Fig. 4a, Δ risk level > 0), where the P fertilization rate is the same to isolate the impact of eCO_2. These areas are distributed globally across rice paddy fields, especially in China and India, which have large areas of rice paddy fields. Relatively speaking, low-income countries[44] (Methods and Extended Data Fig. 9) will suffer more, with 70% of their rice paddy fields projected to face increased yield reduction risks, compared to 52% in middle–high-income countries (Fig. 4b). Middle–high-income countries have substantial concentrations of soil legacy P[45,46] and have better resources for recycling alternative fertilizer P from waste and organic compounds[18,47,48]. Lower P availability under eCO_2 caused a reduction of potential P pollution risk (Fig. 4c, Δ risk level < 0) across 8% of the global rice paddy fields. This reduction was concentrated largely in India, so low-income countries overall benefit more from reduced potential P pollution risk than middle–high-income countries (Fig. 4d). That being said, in low-income countries, the portion of rice paddy fields associated with the enhanced risk for yield reduction was larger than that from reduced P pollution risk under eCO_2 $\left(\frac{\Delta \text{ yield reduction area}}{\Delta \text{P pollution risk area}} = 13.57\right)$. Overall, eCO_2-induced P deficiency threatens the security of future rice supply, although we acknowledge that issues associated with reduced P availability are not the same for all countries. Roughly, to keep a non-negative P balance (P input ≥ P harvest) to avoid reductions in soil available P supply for rice production under eCO_2, P fertilization rates need to increase by more than 100% in countries such as Myanmar and Indonesia (Supplementary Table 4). Hence, to ensure future crop and environmental gains, climate change must be included as a key factor for future sustainable strategies of P management.

Conclusions

Our findings provide evidence that long-term elevated CO_2 in paddy fields will significantly decrease soil available P, which will intensify the risk of P deficiency but alleviate potential P pollution risks from the

https://doi.org/10.1038/s41561-022-01105-y

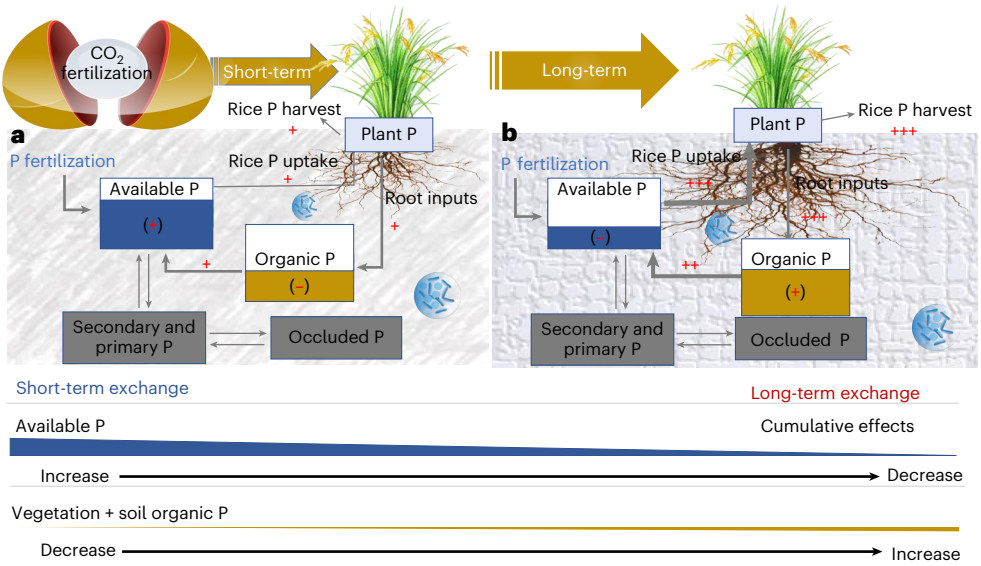

Fig. 3 | Conceptual model illustrating the effects of eCO_2 on soil P pools in paddy soils in the short term and long term. a, Short-term model (≤1 year). **b**, Long-term model (≥9 years). The + and − signs indicate increase and decrease, respectively, in P fluxes or pools. The widths of the arrows and the number of signs (one or multiple + and −) indicate the size of fluxes.

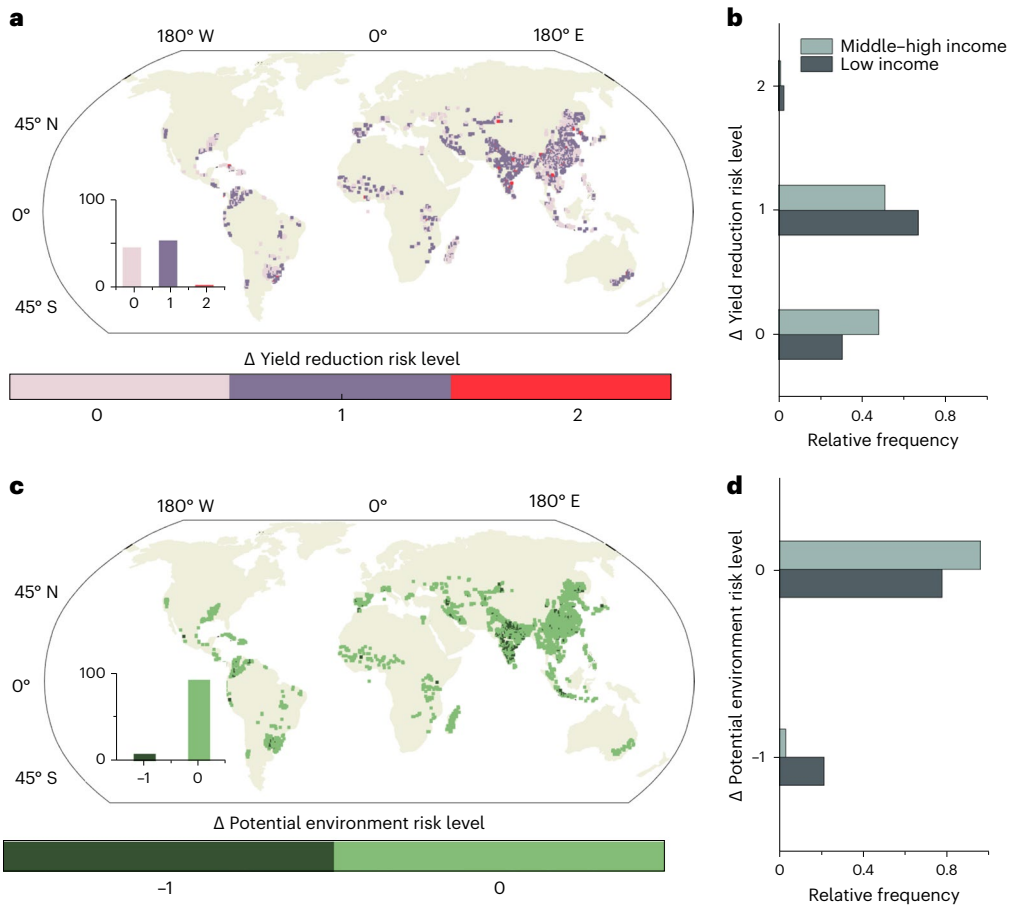

Fig. 4 | Changes in rice yield reduction and potential P pollution risks due to eCO_2. a, Difference (Δ) in yield reduction risk (eCO_2 − aCO_2; 0, the same risk level; 1 and 2, increasing risk levels by 1 and 2). The inset describes the relative frequency of Δ yield reduction risk level. **b**, Relative frequency of Δ yield reduction risk in low- and middle–high-income countries. **c**, Difference (Δ) in potential P pollution risk (−1, no risk to risky; 0, keeps no risk). The inset describes the relative frequency of Δ potential environment risk level. **d**, Relative portion of Δ potential P pollution risk in low- and middle–high-income countries. The size of the squares does not represent the actual area in **a** and **c**.

loss of soil P in high-P croplands. The reduction of soil available P with increases in atmospheric CO_2 is thus a 'double-edged sword'. This situation is likely to place poor countries under more adverse conditions and further widen the economic inequality associated with CO_2 emissions. Global P resources are projected to become more limited in the future[16]. Countries traditionally suffering from P limitation are likely to face more severe future P limitations, exacerbated by increased atmospheric CO_2 concentrations. The phenomenon of progressive available P reduction induced by CO_2 fertilization has been largely overlooked due to a lack of long-term experiments. Our unique long-term rice FACE experiments provide science-based evidence related to plausible predictions about future soil P availability. This research demonstrates the need for further investigations and more long-term experiments from the community to move beyond idealized upscaling, to embrace the real-world complexity and spatial heterogeneity of the effects of climate change and soil, crop and management practices for sustainable food production.

Online content

Any methods, additional references, Nature Portfolio reporting summaries, source data, extended data, supplementary information, acknowledgements, peer review information; details of author contributions and competing interests; and statements of data and code availability are available at https://doi.org/10.1038/s41561-022-01105-y.

References

1. Wang, S. H. et al. Recent global decline of CO_2 fertilization effects on vegetation photosynthesis. *Science* **370**, 1295–1300 (2020).
2. Ainsworth, E. A. & Long, S. P. 30 years of free-air carbon dioxide enrichment (FACE): what have we learned about future crop productivity and its potential for adaptation? *Glob. Change Biol.* **27**, 27–49 (2021).
3. Kimball, B. A. Crop responses to elevated CO_2 and interactions with H_2O, N and temperature. *Curr. Opin. Plant Biol.* **31**, 36–43 (2016).
4. Kim, H. Y. et al. Effects of free-air CO_2 enrichment and nitrogen supply on the yield of temperate paddy rice crops. *Field Crops Res.* **83**, 261–270 (2003).
5. Shimono, H. et al. Rice yield enhancement by elevated CO_2 is reduced in cool weather. *Glob. Change Biol.* **14**, 276–284 (2008).
6. Shimono, H. et al. Genotypic variation in rice yield enhancement by elevated CO_2 relates to growth before heading, and not to maturity group. *J. Exp. Bot.* **60**, 523–532 (2009).
7. Luo, Y. et al. Progressive nitrogen limitation of ecosystem responses to rising atmospheric carbon dioxide. *Bioscience* **54**, 731–739 (2004).
8. Reich, P. B. & Hobbie, S. E. Decade-long soil nitrogen constraint on the CO_2 fertilization of plant biomass. *Nat. Clim. Change* **3**, 278–282 (2013).
9. Ellsworth, D. S. et al. Convergence in phosphorus constraints to photosynthesis in forests around the world. *Nat. Commun.* **13**, 5005 (2022).
10. Brooks, A., Woo, K. C. & Wong, S. C. Effects of phosphorus-nutrition on the response of photosynthesis to CO_2 and O_2, activation of ribulose bisphosphate carboxylase and amounts of ribulose bisphosphate and 3-phosphoglycerate in spinach leaves. *Photosynth. Res.* **15**, 133–141 (1988).
11. Jin, J., Tang, C. X. & Sale, P. The impact of elevated carbon dioxide on the phosphorus nutrition of plants: a review. *Ann. Bot.* **116**, 987–999 (2015).
12. Jin, J. et al. Increased microbial activity contributes to phosphorus immobilization in the rhizosphere of wheat under elevated CO_2. *Soil Biol. Biochem.* **75**, 292–299 (2014).
13. Drissner, D., Blum, H., Tscherko, D. & Kandeler, E. Nine years of enriched CO_2 changes the function and structural diversity of soil microorganisms in a grassland. *Eur. J. Soil Sci.* **58**, 260–269 (2007).
14. He, X. J. et al. Global patterns and drivers of soil total phosphorus concentration. *Earth Syst. Sci. Data* **13**, 5831–5846 (2021).
15. MacDonald, G. K., Bennett, E. M., Potter, P. A. & Ramankutty, N. Agronomic phosphorus imbalances across the world's croplands. *Proc. Natl Acad. Sci. USA* **108**, 3086–3091 (2011).
16. Brownlie, W. J. et al. Global actions for a sustainable phosphorus future. *Nat. Food* **2**, 71–74 (2021).
17. Alewell, C. et al. Global phosphorus shortage will be aggravated by soil erosion. *Nat. Commun.* **11**, 4546 (2020).
18. Penuelas, J. & Sardans, J. The global nitrogen-phosphorus imbalance. *Science* **375**, 266–267 (2022).
19. Obersteiner, M., Penuelas, J., Ciais, P., van der Velde, M. & Janssens, I. A. The phosphorus trilemma. *Nat. Geosci.* **6**, 897–898 (2013).
20. Kogel-Knabner, I. et al. Biogeochemistry of paddy soils. *Geoderma* **157**, 1–14 (2010).
21. Dong, J. W. & Xiao, X. M. Evolution of regional to global paddy rice mapping methods: a review. *ISPRS J. Photogramm. Remote Sens.* **119**, 214–227 (2016).
22. Fu, J. et al. Nationwide estimates of nitrogen and phosphorus losses via runoff from rice paddies using data-constrained model simulations. *J. Clean. Prod.* **279**, 123642 (2021).
23. O'Sullivan, J. B., Jin, J. & Tang, C. X. Elevated CO_2 promotes the acquisition of phosphorus in crop species differing in physiological phosphorus-acquiring mechanisms. *Plant Soil* **455**, 397–408 (2020).
24. Wang, J. Y. et al. Response of rice production to elevated CO_2 and its interaction with rising temperature or nitrogen supply: a meta-analysis. *Clim. Change* **130**, 529–543 (2015).
25. Jin, J., Armstrong, R. & Tang, C. X. Long-term impact of elevated CO_2 on phosphorus fractions varies in three contrasting cropping soils. *Plant Soil* **419**, 257–267 (2017).
26. Jin, J., Tang, C. X., Armstrong, R., Butterly, C. & Sale, P. Elevated CO_2 temporally enhances phosphorus immobilization in the rhizosphere of wheat and chickpea. *Plant Soil* **368**, 315–328 (2013).
27. Jin, J., Tang, C. X., Armstrong, R. & Sale, P. Phosphorus supply enhances the response of legumes to elevated CO_2 (FACE) in a phosphorus-deficient vertisol. *Plant Soil* **358**, 86–99 (2012).
28. Tiessen, H. & Moir, J. O. in *Soil Sampling and Methods of Analysis* (ed. Carter, M. R.) 75–86 (Lewis Publishers, 1993).
29. Helfenstein, J. et al. Combining spectroscopic and isotopic techniques gives a dynamic view of phosphorus cycling in soil. *Nat. Commun.* **9**, 3226 (2018).
30. Hasegawa, T. et al. Rice cultivar responses to elevated CO_2 at two free-air CO_2 enrichment (FACE) sites in Japan. *Funct. Plant Biol.* **40**, 148–159 (2013).
31. Liu, X. et al. Intensification of phosphorus cycling in China since the 1600s. *Proc. Natl Acad. Sci. USA* **113**, 2609–2614 (2016).
32. Hu, M. P. et al. Long-term (1980–2015) changes in net anthropogenic phosphorus inputs and riverine phosphorus export in the Yangtze River basin. *Water Res.* **177**, 115779 (2020).
33. Yang, L. X. et al. Seasonal changes in the effects of free-air CO_2 enrichment (FACE) on growth, morphology and physiology of rice root at three levels of nitrogen fertilization. *Glob. Change Biol.* **14**, 1844–1853 (2008).
34. BassiriRad, H., Gutschick, V. P. & Lussenhop, J. Root system adjustments: regulation of plant nutrient uptake and growth responses to elevated CO_2. *Oecologia* **126**, 305–320 (2001).
35. Gamper, H. et al. Arbuscular mycorrhizal fungi benefit from 7 years of free air CO_2 enrichment in well-fertilized grass and legume monocultures. *Glob. Change Biol.* **10**, 189–199 (2004).
36. Huang, W. J. et al. Shifts in soil phosphorus fractions under elevated CO_2 and N addition in model forest ecosystems in subtropical China. *Plant Ecol.* **215**, 1373–1384 (2014).

37. Khan, F. N., Lukac, M., Turner, G. & Godbold, D. L. Elevated atmospheric CO_2 changes phosphorus fractions in soils under a short rotation poplar plantation (EuroFACE). *Soil Biol. Biochem.* **40**, 1716–1723 (2008).
38. Hasegawa, S., Macdonald, C. A. & Power, S. A. Elevated carbon dioxide increases soil nitrogen and phosphorus availability in a phosphorus-limited Eucalyptus woodland. *Glob. Change Biol.* **22**, 1628–1643 (2016).
39. Li, H. et al. Integrated soil and plant phosphorus management for crop and environment in China. A review. *Plant Soil* **349**, 157–167 (2011).
40. Wang, Y. et al. Response of soil microbes to a reduction in phosphorus fertilizer in rice-wheat rotation paddy soils with varying soil P levels. *Soil Res.* **181**, 127–135 (2018).
41. Zhang, W. F. et al. Efficiency, economics and environmental implications of phosphorus resource use and the fertilizer industry in China. *Nutr. Cycl. Agroecosyst.* **80**, 131–144 (2008).
42. Hesketh, N. & Brookes, P. C. Development of an indicator for risk of phosphorus leaching. *J. Environ. Qual.* **29**, 105–110 (2000).
43. Fortune, S., Lu, J., Addiscott, T. M. & Brookes, P. C. Assessment of phosphorus leaching losses from arable land. *Plant Soil* **269**, 99–108 (2005).
44. Hamadeh, N., Rompaey, C. V. & Metreau, E. New World Bank country classifications by income level: 2021–2022. *World Bank Blogs* https://blogs.worldbank.org/opendata/new-world-bank-country-classifications-income-level-2021-2022 (2021).
45. Zhang, J. et al. Spatiotemporal dynamics of soil phosphorus and crop uptake in global cropland during the twentieth century. *Biogeosciences* **14**, 2055–2068 (2017).
46. Mogollón, J. M., Beusen, A., Grinsven, H. V., Westhoek, H. & Bouwman, A. F. Future agricultural phosphorus demand according to the shared socioeconomic pathways. *Glob. Environ. Change* **50**, 149–163 (2018).
47. Campos, J. L. et al. Nitrogen and phosphorus recovery from anaerobically pretreated agro-food wastes: a review. *Front. Sustain. Food Syst.* **2**, 91 (2019).
48. Mogollon, J. M. et al. More efficient phosphorus use can avoid cropland expansion. *Nat. Food* **2**, 509–518 (2021).

[1]State Key Laboratory of Soil and Sustainable Agriculture, Institute of Soil Science, Chinese Academy of Sciences, Nanjing, China. [2]CSIRO Oceans and Atmosphere, Aspendale, Victoria, Australia. [3]Key Laboratory of Surficial Geochemistry, Ministry of Education, School of Earth Sciences and Engineering, Nanjing University, Nanjing, China. [4]Key Lab of Urban Environment and Health, Institute of Urban Environment, Chinese Academy of Sciences, Xiamen, China. [5]Research Center for Eco-Environmental Sciences, Chinese Academy of Sciences, Beijing, China. [6]Department of Renewable Resources, University of Alberta, Edmonton, Alberta, Canada. [7]School of Integrative Plant Science, Cornell University, Ithaca, NY, USA. [8]Laboratoire des Sciences du Climat et de l'Environnement, LSCE/IPSL, CEA-CNRS-UVSQ, Université Paris-Saclay, Gif-sur-Yvette, France. [9]CSIC, Global Ecology Unit CREAF-CSIC-UAB, Bellaterra, Spain. [10]CREAF, Cerdanyola del Vallès, Spain. [11]Adaptive Cropping Systems Laboratory, US Department of Agriculture, Agricultural Research Service, Beltsville, MD, USA. [12]Swift Current Research and Development Centre, Agriculture and Agri-Food Canada, Swift Current, Saskatchewan, Canada. [13]Department of Entomology and Plan Pathology, North Carolina State University, Raleigh, NC, USA. [14]Nanjing Institute of Environmental Sciences, Ministry of Ecology and Environment, Nanjing, China. [15]School of Fisheries, Aquaculture and Aquatic Sciences, Auburn University, Auburn, AL, USA. [16]State Key Laboratory of Pollution Control and Resource Reuse, School of the Environment, Nanjing University, Nanjing, China. [17]Tourism College, Henan Normal University, Xinxiang, China. [18]These authors contributed equally: Yu Wang, Yuanyuan Huang. ✉e-mail: cwzhu@issas.ac.cn

Methods

The China rice FACE field experiments

Study $P_{L\text{-}M}$. This rice FACE experiment was initiated in June 2004 and was conducted in a typical Chinese rice-growing region with a subtropical monsoon climate (Supplementary Fig. 1; Jiangdu FACE, Zhongcun Village, 32° 35′ 5″ N, 119° 42′ 0″ E, Yangzhou City, Jiangsu, China). The FACE experiment consisted of three identical octagonal rings (14 m in diameter) receiving a CO_2 concentration of 200 µmol mol^{-1} above the ambient concentration (eCO_2) and three rings with ambient atmospheric CO_2 (aCO_2) as the control. The FACE platform followed the method of ref. [49], using compressed and pure CO_2 from release tubes surrounding the rice plot. The average daytime [CO_2] in 2018 (in the rice-growing season) varied between 588 and 601 µmol mol^{-1}, and the ambient [CO_2] was 393 µmol mol^{-1}. As described in ref. [50], the soil is classified as a Shajiang aquic cambisol with a sandy loamy texture and a pH of 6.82, an organic carbon (C) content of 1.84%, and total nitrogen (N) and phosphorus (P) of 1.45 g kg^{-1} and 0.63 g kg^{-1}, respectively, and characterized by a low to moderate concentration (10.1 mg kg^{-1}) of Olsen P (study $P_{L\text{-}M}$). The crops were managed with agronomic practices commonly used in this region. Rice seeds (*Oryza sativa* cv.) were sown in mid to late May, and seedlings were transplanted in mid to late June of each year. Fertilizers were applied as a compound fertilizer ($N:P_2O_5:K_2O$ = 15:15:15 (%), basal dressing) and urea (N, 46%, top dressing), at rates of 250 kg N ha^{-1}, 31 kg P ha^{-1} and 58 kg potassium (K) ha^{-1} during 2004–2012 (Supplementary Table 5). The N application rate decreased to 225 kg ha^{-1}, and the P and K rates increased to 39 and 75 kg ha^{-1}, respectively, during 2013–2018. For all seasons, N was applied as a basal dressing (40%), and as a top dressing at early tillering (30%) and at the panicle initiation stage (30%). All applications of P and K were basal dressings.

Study P_H. This rice FACE experiment was established in April 2011 and was conducted in a typical Chinese rice-growing region with a subtropical monsoon climate (Supplementary Fig. 1, Kangbo Village, 31° 30′ N, 120° 33′ E, Changshu City, Jiangsu, China). As described in ref. [51], the soil is a gleyic stagnic anthrosol formed on a clayey lacustrine deposit with a pH of 7.0, organic C content of 1.60%, and total N and P of 1.90 g kg^{-1} and 0.90 g kg^{-1}, respectively. This experiment (study P_H) was conducted in a paddy soil with a high concentration (22.2 mg kg^{-1}) of Olsen P. Rice and winter wheat were rotated at this site. This FACE platform followed the method of ref. [49]. The eCO_2 target was 100 µmol mol^{-1} above ambient during 2011–2018, and 200 µmol mol^{-1} above ambient in 2019. The average daytime [CO_2] in 2019 varied between 590 and 624 µmol mol^{-1}, and the ambient [CO_2] was 405 µmol mol^{-1}. Each treatment was replicated in three rings with the same infrastructure. Nitrogen fertilizer was applied in each season at a rate of 181 kg N ha^{-1}, with 40% of the total as a basal fertilizer before the seedlings were transplanted, 30% as a top dressing at early tillering and 30% at the panicle initiation stage. Calcium superphosphate (26 kg P ha^{-1}) and potassium chloride (100 kg K ha^{-1}) were applied as for the basal fertilizers (Supplementary Table 5).

Sampling and analysis

Soil samples were collected at the rice ripening stage in 2004 (year 1), 2009 (year 6), 2015 (year 12) and 2018 (year 15) in study $P_{L\text{-}M}$, and in 2019 (year 9) in study P_H. In each ring, five soil cores (2.5 cm diameter × 20 cm deep) were sampled and pooled into a single sample, air-dried, ground, sieved (<2-mm sieve) and stored at room temperature for chemical analysis. Biomass and total P concentrations including rice straw and grain were measured in 2018 (study $P_{L\text{-}M}$) and 2019 (study P_H). Soil P balance was calculated as the difference between P input through fertilizer and P removed through crop harvest[52]. Crop total P was determined by digestion with sulfuric acid (H_2SO_4) and hydrogen peroxide (H_2O_2), followed by colorimetric analysis with an ultraviolet spectrometer (UVmini-1240, Shimadzu)[53].

Sequential chemical extraction of soil P

A modified Hedley method[28,54] fractionation procedure was used to estimate soil P pools of different solubilities. The modification categorizes soil microbial biomass P as part of the $NaHCO_3$–P fraction (instead of an individual P pool) and aggregate P as part of the NaOH–P fraction (instead of an individual P pool). Briefly, P was fractionated into five pools, including resin–P (extracted with deionized water and anion exchange resin), $NaHCO_3$–P_i and $NaHCO_3$–P_o (extracted with 0.5 M $NaHCO_3$), NaOH–P_i and NaOH–P_o (extracted with 0.1 M NaOH), HCl–P_i (extracted with 1 M HCl) and residual-P (digested with H_2SO_4 and H_2O_2). Available P was calculated as the sum of resin–P and $NaHCO_3$–P_i. Primary and secondary mineral P refer to HCl–P_i and NaOH–P_i, respectively. Organic P (P_o) was the sum of $NaHCO_3$–P_o and NaOH–P_o. $NaHCO_3$–P_o was calculated from the difference between $NaHCO_3$–total P (from digestion) and $NaHCO_3$–P_i. NaOH–P_o was calculated from the difference between NaOH–total P (from digestion) and NaOH–P_i. Residual P indicated the occluded P pool. The P concentration in each extract was determined by measuring absorbance at 700 nm using a UVmini-1240 ultraviolet spectrophotometer (Shimadzu) using the ascorbic acid molybdenum blue method. Available plant P was also quantified using the Olsen P test as the traditional index, using sodium bicarbonate ($NaHCO_3$, pH 8.5) as the extractant[55].

^{31}P solid-state NMR spectroscopy and ^{31}P liquid NMR spectroscopy

Solid-state ^{31}P single pulse magic-angle-spinning (MAS) NMR spectra were collected for four soil samples from the aCO_2 and eCO_2 treatments in year 15 in study P_H and year 9 in study $P_{L\text{-}M}$ using a 400-MHz Bruker AVIII solid-state spectrometer (9.4 T), at an operating frequency of 168.1 MHz for ^{31}P. A Bruker 4.0-mm HX double-resonance probe was used for all solid-state NMR measurements. For the ^{31}P solid-state NMR, soil samples were ground to fine powders and then packed into a ZrO rotor (outer diameter, 4 mm). Spectra were acquired at a MAS spinning rate of 10 kHz using a ^{31}P 30° pulse length of 1.5 µs and a relaxation delay of 30 s. We collected more than ~3,000 scans for each sample, depending on signal sensitivity. The ^{31}P chemical shifts ($\delta_{P\text{-}31}$) are reported relative to an external 85% H_3PO_4 solution at $\delta_{P\text{-}31}$ = 0 ppm. A dominant peak at ~2.6 ppm was clearly observed and can be assigned to an apatite group mineral (primary P, calcium phosphate (Ca–PO_4) mineral)); all Ca–PO_4 minerals yield chemical shifts at −2 to 3 ppm (ref. [56]). For solution ^{31}P NMR, soils were extracted with NaOH–EDTA, which recovered 50.3–60.4% of the total P[57]. Spectra of extracted soil samples were collected using a Bruker 400-MHz solution NMR spectrometer operating at 161.8 MHz for ^{31}P with a 10-mm Broadband Observe at 25 °C, and a 45° radiofrequency pulse (zgig pulse program), an acquisition time of 0.845 s, a recycle delay time of 4 s, and 5,000 to 10,000 scans. The chemical shifts of soil P compounds were classified according to ref. [58]. The relative abundance of each class was estimated as the relative percentage of integral area of the corresponding region to the total spectral area using the standard TopSpin software (Bruker) and MestRenova.

Soil microbial analysis

The soil microbial community composition was determined using a phospholipid fatty acid analysis as described in ref. [59], with slight modifications. Briefly, phospholipid fatty acids were extracted from freeze-dried soil samples with a single-phase mixture of a chloroform–methanol–citrate buffer (1:2:0.8, vol:vol:vol; 0.15 M, pH 4.0). The resulting fatty-acid methyl esters were then separated and identified using an Agilent 7890N gas chromatograph fitted with a MIDI Sherlock microbial identification system (version 4.5). The fatty acids i14:0, i15:0, a15:0, i16:0, 16:1w7c, i17:0, a17:0, 17:0cy, 18:1w9, 18:1w7c and 19:0cy were used as bacterial markers, and 18:1w9c and 18:2w6.9c were used as fungal markers. The fatty acid 16:1w5c was used as the marker for AMF. The ACP and ALP activities were measured using *p*-nitrophenyl phosphate (Sigma-Aldrich) as the substrate[60].

Imaging rice roots

The rice roots were imaged in situ at the heading stage for the eCO_2 and aCO_2 treatments from the P_H experiment. In detail, a root tube 1 m in length was buried at an angle of 45° between two rice rows, with 60 cm of the length underground (~42-cm vertical depth), to obtain root images using a CI-600 In-Situ Root Imager (CID Bio-Science), and the images were analysed using CI-600 software.

Changes of soil available P in different agroecosystems

We compiled a worldwide database to assess the influence of eCO_2 on available P in comparison with aCO_2. We identified potential published studies in the Web of Science online reference database with the keywords 'elevated CO_2 and P availability' or 'elevated CO_2 and P fraction' (accessed February 2022). We only selected publications that reported the response of Olsen-P or P fractions to eCO_2 concentrations, and 14 studies met the criteria. The experimental type, cultivation duration, ecosystem and soil available P are summarized in Supplementary Table 1. The ecosystem mainly includes three types: forest, grassland and farmland (Extended Data Fig. 7).

Soil available P across global rice fields under eCO_2

The distribution of soil available P across global rice fields was derived from data from ref. [61], which was downloaded as a 0.5° × 0.5° grid from the European Soil Data Centre (source, https://esdac.jrc.ec.europa.eu/content/global-phosphorus-losses-due-soil-erosion; accessed 20 April 2021[62,63]). This global dataset of soil P was generated for agricultural soils by combining different data sources that used the Hedley fractionation method. The spatial resolution of the data is 0.5° × 0.5°. This global dataset provides estimated cropland P pools for 2005, with soil P budget terms derived from farming practices and atmospheric deposition. As a coarse approximation, we estimated the change in soil available P across global rice fields that would occur under eCO_2, by deriving a spatially constant response ratio from our FACE results and applying it to the ref. [61] P data. Here, the P fertilization rate is the same under aCO_2 and eCO_2 to isolate the impact of eCO_2.

The risk levels of P deficiency and environmental pollution were classified using the Olsen-P concentration based on previous studies[39–43]. Rice yield reduction risk is categorized as follows: level 5: extremely high risk of yield reduction, Olsen P < 5 mg kg^{-1}; level 4: high risk of yield reduction, 5 ≤ Olsen P < 10 mg kg^{-1}; level 3: medium risk of yield reduction, 10 ≤ Olsen P < 20 mg kg^{-1}; level 2: low risk of yield reduction, 20 ≤ Olsen P < 30 mg kg^{-1}; level 1: extremely low risk of yield reduction, 30 ≤ Olsen P < 40 mg kg^{-1}. Environmental pollution risk is categorized as follows: level 1: potential P pollution risk, Olsen P ≥ 40 mg kg^{-1}; level 0: potential P pollution risk, Olsen P < 40 mg kg^{-1}.

The thresholds for the concentrations of available P were then calculated using the relationship between Olsen P and available P concentrations as shown in Extended Data Fig. 10. Olsen P concentrations of 5, 10, 20, 30 and 40 mg kg^{-1} corresponded to soil available P concentrations of 14, 20, 30, 40 and 50 mg kg^{-1}, respectively. Global spatial distribution results for current and future yield reduction level and potential environment risk level were then derived based on the current and future soil available P content and the thresholds.

We then quantified yield reduction and potential P pollution risks across 14 main rice-growing nations, and assessed the risks against national wealth; the latter was based on per capita gross national product during the period 2010–2020[44] (Extended Data Fig. 9). We divided these 14 nations into low- and middle–high-income groups using a threshold value of 4,046 US$ gross domestic product per capita, based on World Bank income classifications[44]. The low-income countries in this study include Cambodia, Pakistan, Myanmar, Bangladesh, India, Vietnam, Philippines and Indonesia. The middle–high-income countries include Thailand, China, Brazil, America, South Korea and Japan.

Statistical analysis

We used analysis of variance with repeated measures to compare differences between ambient and elevated CO_2 treatments with time in the $P_{L\text{-}M}$ FACE experiment, and analysis by Tukey's test to compare differences between ambient and elevated CO_2 treatments in the P_H FACE experiment. All statistical analyses were performed using SPSS 16.0 software (SPSS). Pearson correlation coefficients were calculated to analyse the relationship between microbial biomass, enzyme activities and the distribution of P.

Data availability

The data supporting the findings of this study are available within the Article and the Supplementary Information, and we have deposited the global dataset in the figshare repository (https://doi.org/10.6084/m9.figshare.21103078.v2 ref. [64]). Global rice yield data of the 14 main rice-planting countries can be accessed from FAOSATA (http://faostat.fao.org/default.aspx, 2019). Global rice harvest area data for extracting global rice pixels are available from https://www.mapspam.info/data/. Global soil P pools and P budgets can be accessed at https://esdac.jrc.ec.europa.eu/content/global-phosphorus-losses-due-soil-erosion.

Code availability

Code used in data processing and figure generation is provided through https://doi.org/10.6084/m9.figshare.21098458.v2 (ref. [65]).

References

49. Okada, M. et al. Free-air CO_2 enrichment (FACE) using pure CO_2 injection: system description. *N. Phytol.* **150**, 251–260 (2001).
50. Zhu, C. W. et al. The temporal and species dynamics of photosynthetic acclimation in flag leaves of rice (*Oryza sativa*) and wheat (*Triticum aestivum*) under elevated carbon dioxide. *Physiol. Plant.* **145**, 395–405 (2012).
51. Cai, C. et al. Responses of wheat and rice to factorial combinations of ambient and elevated CO_2 and temperature in FACE experiments. *Glob. Change Biol.* **22**, 856–874 (2016).
52. Nagumo, T., Tajima, S., Chikushi, S. & Yamashita, A. Phosphorus balance and soil phosphorus status in paddy rice fields with various fertilizer practices. *Plant Prod. Sci.* **16**, 69–76 (2013).
53. Kovar, J. L. & Pierzynski, G. M. (eds) *Methods of Phosphorus Analysis for Soils, Sediments, Residuals and Waters* 2nd edn (North Carolina State Univ., 2009).
54. Hedley, M. J. & Stewart, J. W. B. Method to measure microbial phosphate in soils. *Soil Biol. Biochem.* **14**, 377–385 (1982).
55. Lu, R. K. *The Analysis Method of Soil Agro-Chemistry* (Chinese Agricultural Academic Press, 2000).
56. Li, W. et al. Characterizing phosphorus speciation of Chesapeake Bay sediments using chemical extraction, ^{31}P NMR, and X-ray absorption fine structure spectroscopy. *Environ. Sci. Technol.* **49**, 203–211 (2015).
57. Chen, S. et al. The influence of long-term N and P fertilization on soil P forms and cycling in a wheat/fallow cropping system. *Geoderma* **404**, 115274 (2021).
58. Cade-Menun, B. J. Characterizing phosphorus in environmental and agricultural samples by ^{31}P nuclear magnetic resonance spectroscopy. *Talanta* **66**, 359–371 (2005).
59. Frostegard, A., Tunlid, A. & Baath, E. Phospholipid fatty acid composition, biomass, and activity of microbial communities from two soil types experimentally exposed to different heavy metals. *Appl. Environ. Microbiol.* **59**, 3605–3617 (1993).
60. Alef, K. & Nannipieri, P. (eds) *Methods in Applied Soil Microbiology and Biochemistry* (Academic Press, 1995).
61. Ringeval, B. et al. Phosphorus in agricultural soils: drivers of its distribution at the global scale. *Glob. Change Biol.* **23**, 3418–3432 (2017).

62. Pariasca-Tanaka, J. et al. Does reducing seed-P concentrations affect seedling vigor and grain yield of rice? *Plant Soil* **392**, 253–266 (2015).
63. European Soil Data Centre (ESDAC, European Commission, Joint Research Centre); esdac.jrc.ec.europa.eu
64. Song, L. Source data for MS: reduced phosphorus availability in paddy soils under atmospheric CO_2 enrichment. figshare https://doi.org/10.6084/m9.figshare.21103078.v2 (2022).
65. Song, L. MS_NG_CFE reduced soil P availability. figshare https://doi.org/10.6084/m9.figshare.21098458.v2 (2022).
66. Yang, L. X. et al. Seasonal changes in the effects of free-air CO_2 enrichment (FACE) on dry matter production and distribution of rice (*Oryza sativa L.*). *Field Crops Res.* **98**, 12–19 (2006).
67. Liu, H. J. et al. Yield formation of CO_2-enriched hybrid rice cultivar Shanyou 63 under fully open-air field conditions. *Field Crops Res.* **108**, 93–100 (2008).
68. Fan, G. Z. et al. Yield components and its conformation responded to elevated atmospheric CO_2 in three rice (*Oryza sativa L.*) generations. *Afr. J. Biotechnol.* **9**, 2118–2124 (2010).
69. Zhu, C. W. et al. Biochemical and molecular characteristics of leaf photosynthesis and relative seed yield of two contrasting rice cultivars in response to elevated CO_2. *J. Exp. Bot.* **65**, 6049–6056 (2014).
70. Lai, S. K. et al. Effects of CO_2 concentration, nitrogen supply and transplanting density on yield formation of hybrid rice Shanyou 63: a FACE study. *J. Agro Environ. Sci.* **33**, 836–843 (2014).
71. Wang, W. L. et al. Elevated CO_2 cannot compensate for japonica grain yield losses under increasing air temperature because of the decrease in spikelet density. *Eur. J. Agron.* **99**, 21–29 (2018).
72. Zhang, G. Y. et al. Grain growth of different rice cultivars under elevated CO_2 concentrations affects yield and quality. *Field Crops Res.* **179**, 72–80 (2015).
73. Hasegawa, T. et al. A High-yielding rice cultivar 'Takanari' shows no N constraints on CO_2 fertilization. *Front Plant Sci.* **10**, 15 (2019).
74. Lieffering, M., Kim, H. Y., Kobayashi, K. & Okada, M. The impact of elevated CO_2 on the elemental concentrations of field grown rice grains. *Field Crops Res.* **88**, 279–286 (2004).
75. Wang, J. Q. et al. Changes in nutrient uptake and utilization by rice under simulated climate change conditions: A 2-year experiment in a paddy field. *Agr. For. Meteorol.* **250**, 202–208 (2018).
76. He, S. D. *Studies on Phosphorus Fractions and Phosphate Sorption Desorption Characteristics of Paddy Soils* [D]. Zhejiang Univ. (2008).
77. Wang, Y. Z. *Effect of Phosphorus Fertilization on Soil Phosphorus Fraction, Distribution and Dynamics* [D]. Univ. Chinese Academy of Sciences (2015).
78. Waqas, A. *Effect of Long-term Fertilization and Tillage Management on Soil Phosphorus Fractions under Paddy Cultivation in Different Agroclimatic Regions of China* [D]. Chinese Academy of Agricultural Sciences (2019).
79. Li, L. *Speciation, Microbial Enzymatic Conversion and Activation of Legacy Phosphorus in Paddy Soils* [D]. Zhejiang Univ. (2014).
80. Wang, X. *Effects of Earthworms on Soil Nitrogen and Phosphorus in Upland Rice-Wheat Rotation Agroecosystem* [D]. Nanjing Agricultural Univ. (2005).
81. Wang, Y. et al. Soil phosphorus pool evolution and environmental risk prediction of paddy soil in the Taihu Lake Region. *Acta Pedologica Sin.* **59**, 1640–1649 (2022) .

Acknowledgements

We acknowledge the enduring contributions of J. Zhu, who initiated and supervised study $P_{L\text{-}M}$ from 2004 to 2016, and G. Pan and X. Liu who established and supervised study P_H from 2011. The FACE system instruments of study $P_{L\text{-}M}$ were supplied by the National Institute of Agro-Environmental Sciences and the Agricultural Research Center of Tohohu Region (Japan). We received funding from the Key-Area Research and Development Program of Guangdong Province, China (2020B0202010006 to C.Z.), the National Key Research and Development Program of China (2021YFD1700802 to Y.W.), the National Natural Science Foundation of China (42277026 to Y.W., 31870423 to C.Z. and 32001191 to L.S.), the Chinese Academy of Sciences '0-1' program (ZDBS-LY-DQC020 to C.Z.), the Jiangsu Science and Technology Department (BM2022002 to C.Z.), Innovation Program of Institute of Soil Science (ISSASIP2201 to Y.W.), a Spanish Government grant (PID2019-110521GB-I00 to J.P.), French state aid managed by the ANR under the 'Investissements d'avenir' programme (ANR16-CONV-0003 to P.C.), and the Carbon Peaking and Carbon Neutrality Special Fund for Science and Technology from Nanjing Science and Technology Bureau (20221103 to C.Z.).

Author contributions

Conceptualization was provided by C.Z., Yu Wang and Y.H., methodology by C.Z., Yu Wang, Y.H., J.Y., L.S., W.L., J.Z., Y.T. and G.L., investigations by C.Z., Yu Wang and Y.H., data curation by Yu Wang, Y.H., J.Y., L.S. and W.L., and formal analysis by Yu Wang, Y.H., J.Y., L.S., J.P. and S.X.C. Supervision was provided by C.Z. and Yu Wang. The original draft was written by Yu Wang, Y.H., L.S. and C.Z. The paper was reviewed and edited by Yu Wang, Y.H., L.S., S.X.C., Y.Z., Y.L., P.C., J.P., J.W., B.J.C.-M., S.H., D.W., Z.Y., Yujun Wang, S.W., X.Y. and C.Z.

Competing interests

The authors declare no competing interests.

Additional information

Extended data is available for this paper at https://doi.org/10.1038/s41561-022-01105-y.

Supplementary information The online version contains supplementary material available at https://doi.org/10.1038/s41561-022-01105-y.

Correspondence and requests for materials should be addressed to Chunwu Zhu.

Peer review information *Nature Geoscience* thanks David Ellsworth and the other, anonymous, reviewer(s) for their contribution to the peer review of this work. Primary Handling Editor: Xujia Jiang, in collaboration with the *Nature Geoscience* team.

https://doi.org/10.1038/s41561-022-01105-y

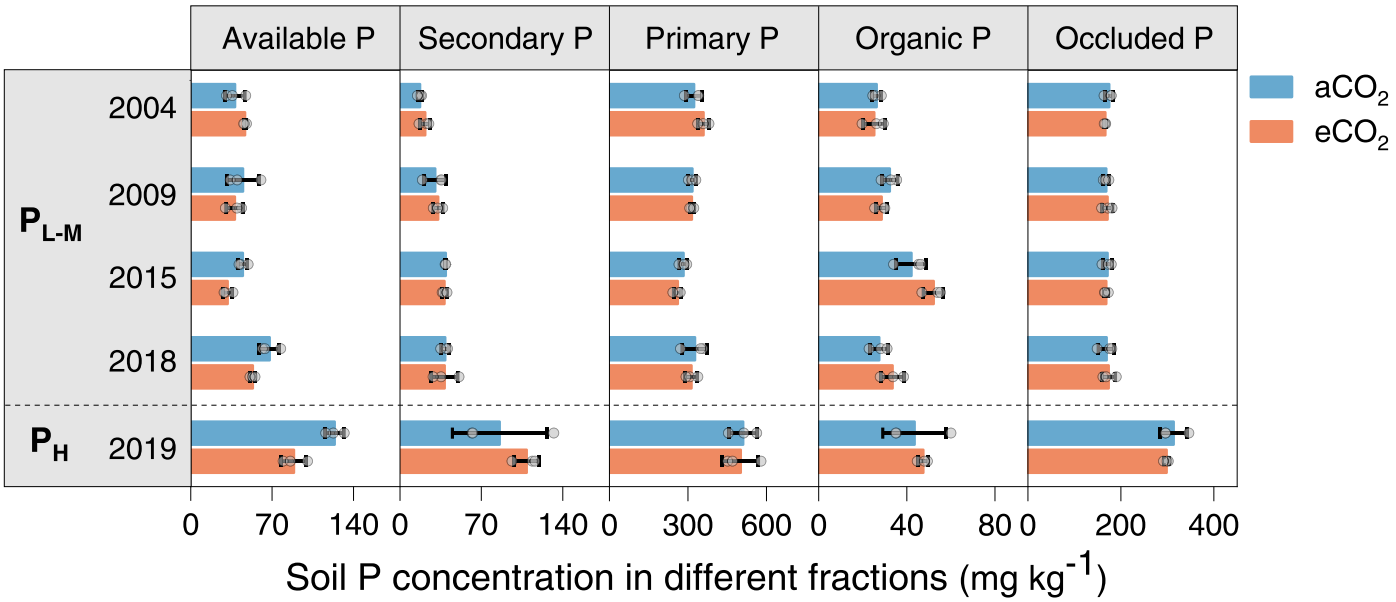

Extended Data Fig. 1 | Variations of soil P factions under eCO_2 and aCO_2 in two China Rice FACE experiments. The samples were collected at the rice harvest stage in agroecosystem with low-moderate P (P_{L-M}) in 2004, 2009, 2015 and 2018, respectively. The high P (P_H) agroecosystem samples were collected at the rice harvest stage in 2019. Data are means ± standard deviation (n = 3). P_{L-M} and P_H were initiated in 2004 and 2011, respectively. Statistical test results are provided in Table 1 and Supplementary Table 2.

https://doi.org/10.1038/s41561-022-01105-y

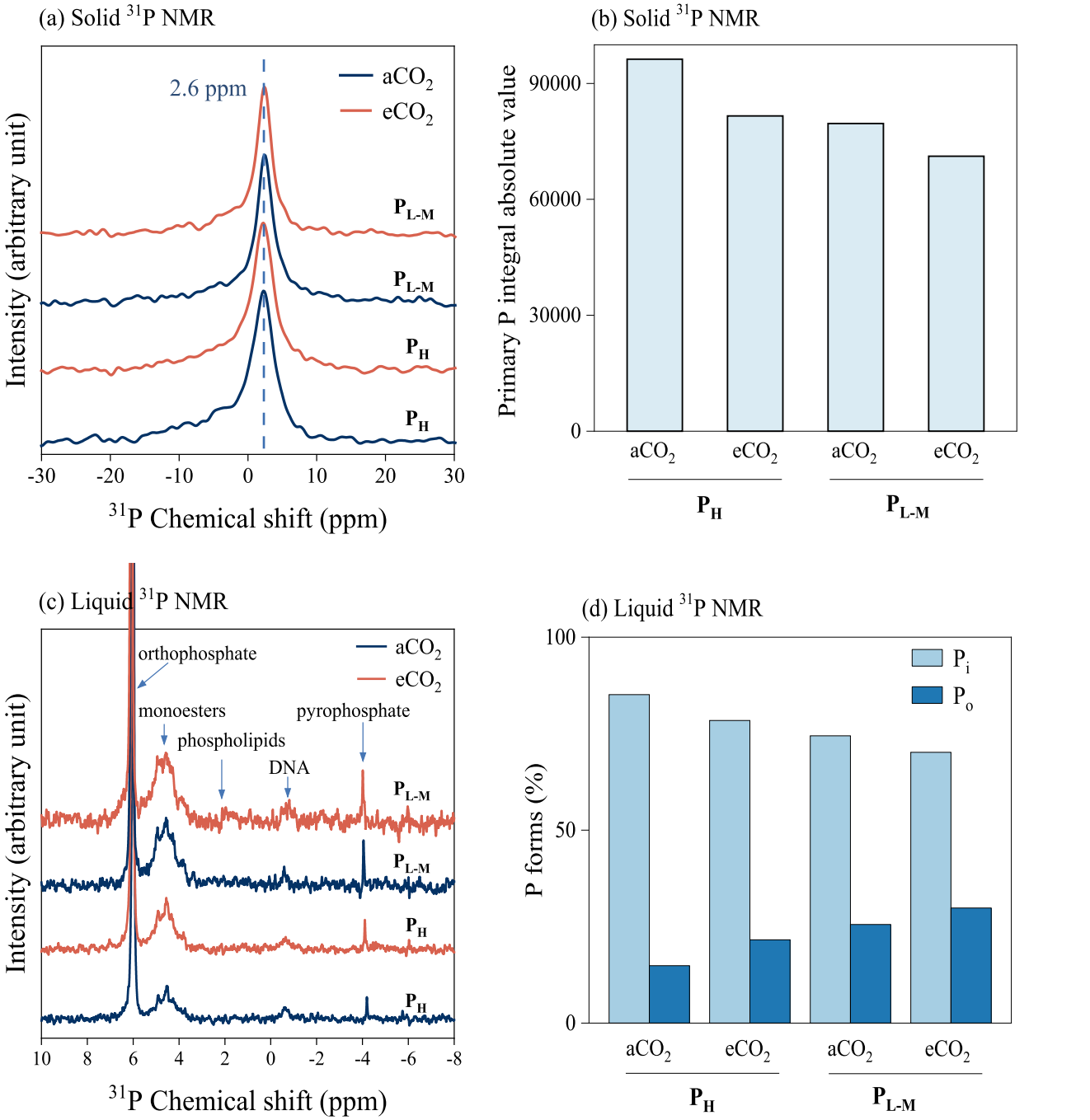

Extended Data Fig. 2 | Variations of ^{31}P NMR spectra under elevated atmospheric CO_2 (eCO_2) in comparison with ambient CO_2 (aCO_2) concentrations in two China Rice FACE experiments. a. b, ^{31}P solid-state NMR spectra in 2018 ($P_{L\text{-}M}$) and 2019 (P_H) at the 0-10 cm soil layer. The peak at 2.6 ppm is indicative of apatite (Ca – P mineral, primary mineral P). **c. d**, ^{31}P liquid-state NMR spectra in 2018 ($P_{L\text{-}M}$) and 2019 (P_H) at the 0-10 cm soil layer. The ^{31}P NMR chemical shifts suggest the presence of orthophosphate (6 ppm), phosphate monoesters (4-5 ppm), phospholipids (1-2.5 ppm), DNA (-1 ppm), and pyrophosphate (-4 to -5 ppm); P_i in **d** refers to the sum of inorganic ortho-P and pyrophosphate, P_o refers to the sum of phosphate monoesters and diester (mainly DNA-P). $P_{L\text{-}M}$ and P_H were initiated in 2004 and 2011, respectively.

https://doi.org/10.1038/s41561-022-01105-y

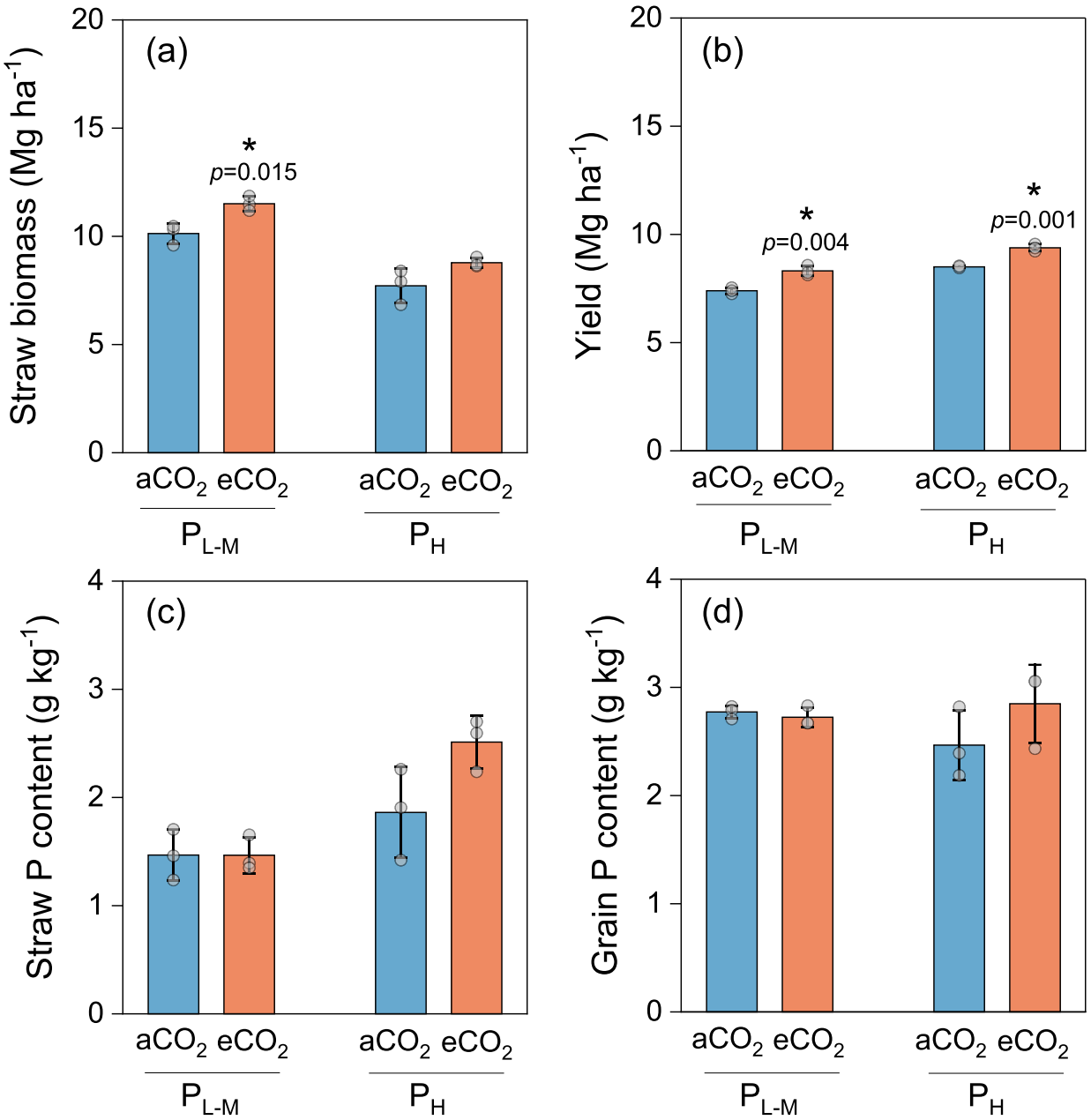

Extended Data Fig. 3 | Straw biomass, grain yield, straw P content and grain P content under aCO_2 and eCO_2 in two rice FACE experiments. Data were collected in 2018 from a low-moderate P (P_{L-M}) agroecosystem, and in 2019 from a high P (P_H) agroecosystem. Data are means ± standard deviation (n = 3). Asterisks denote the results of ANOVA and Tukey tests, and indicate significant differences between means at $p < 0.05$.

https://doi.org/10.1038/s41561-022-01105-y

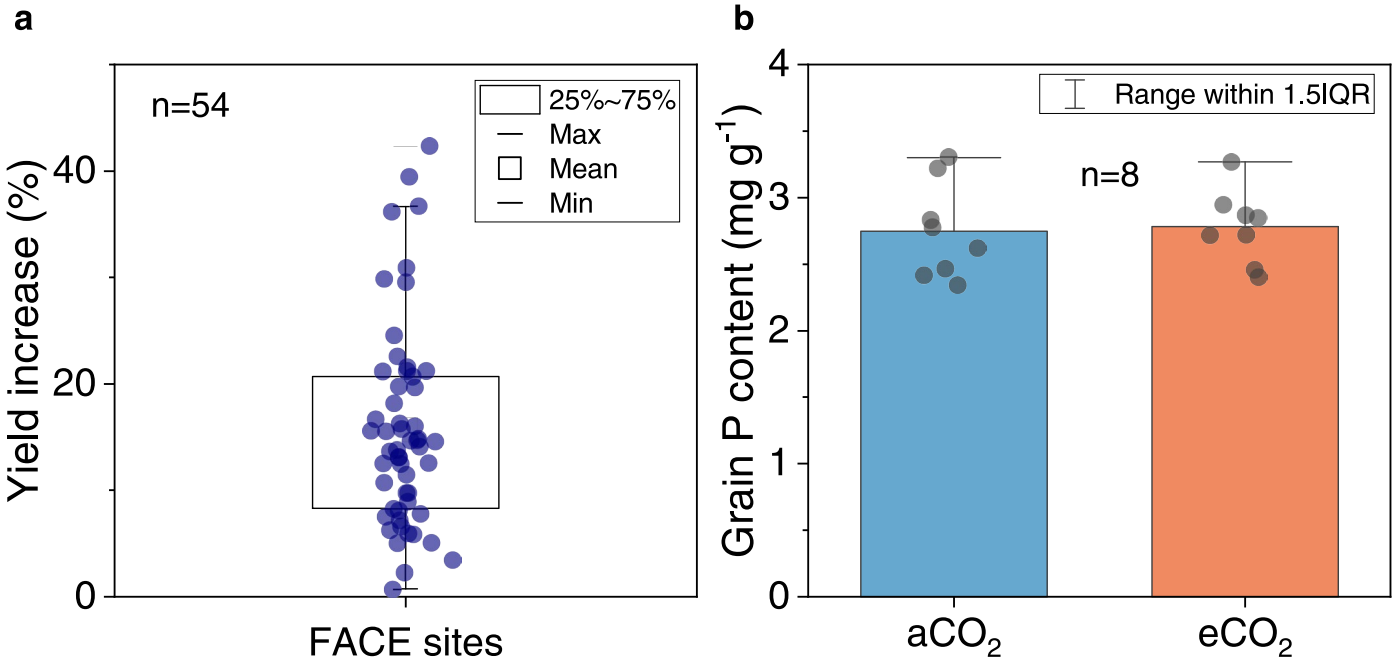

Extended Data Fig. 4 | Rice yield and grain P content response to elevated CO_2. Dots indicate results of FACE experiments in Wuxi, Jiangdu, Changshu, Tsukuba, and Shizukuishi. The IQR indicates the interquartile range. The data are from references[4,6,30,51,66–75].

https://doi.org/10.1038/s41561-022-01105-y

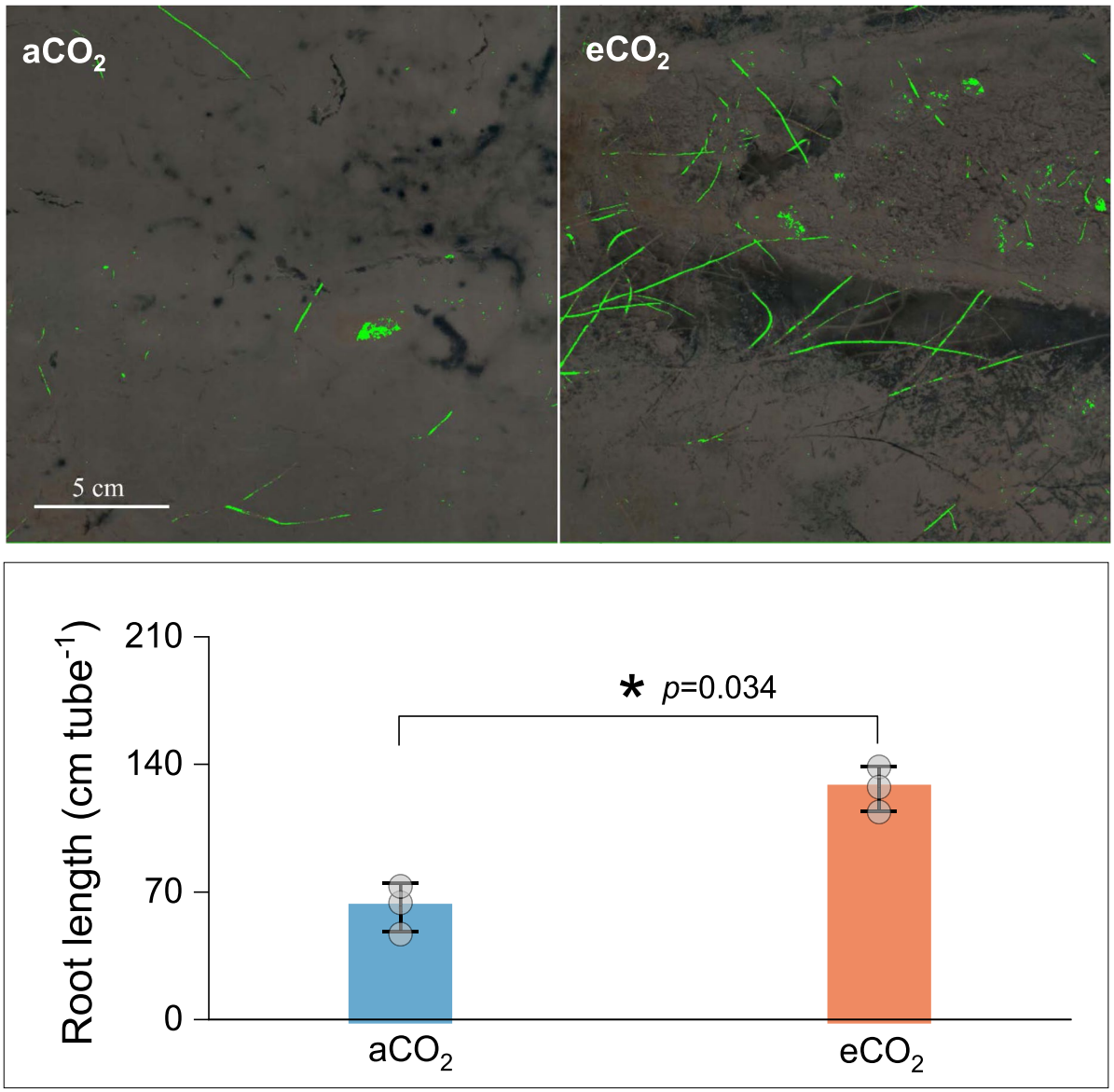

Extended Data Fig. 5 | *In-situ* images of rice roots at the heading stage in agroecosystems in high available P experiment. The image on the left is for the aCO_2 treatment, and the image on the right is for the eCO_2 treatment. Data are means ± standard deviation (n = 3). Asterisks denote the results of ANOVA and Tukey tests, and indicate significant differences between means at $p < 0.05$.

https://doi.org/10.1038/s41561-022-01105-y

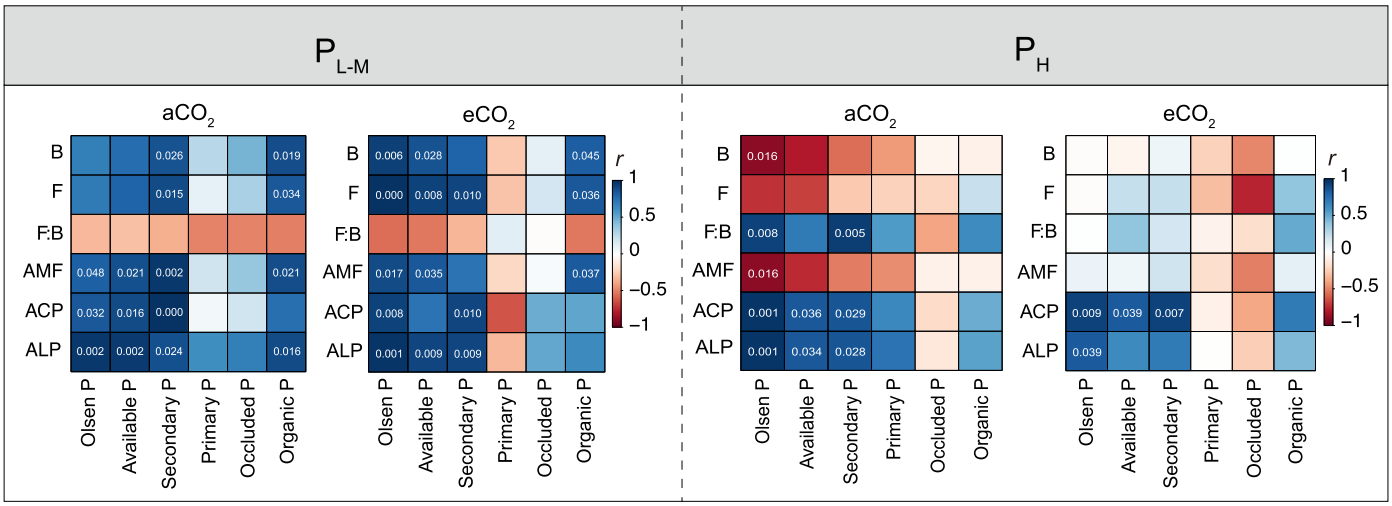

Extended Data Fig. 6 | Relationships between soil P fractions and microbial properties (Pearson correlation coefficients, *r*) under aCO_2 and eCO_2 in 2018 ($P_{L\text{-}M}$) and 2019 (P_H). The values of *p* denote the results of ANOVA and Tukey tests, and described the significance for $p < 0.05$, $p < 0.01$, and $p < 0.001$. Soil available P, the sum of resin-P and $NaHCO_3$-P_i; Secondary mineral P, NaOH-P_i; Primary mineral P, HCl-P_i; Organic P, the sum of $NaHCO_3$-P_o and NaOH-P_o; Occluded P, residual P. Soil microbial properties include bacterial biomass (B), fungal biomass (F), the ratio of fungal to bacteria biomass (F:B ratio), biomass of arbuscular mycorrhizal fungi (AMF), and the activities of acid phosphatase (ACP), and alkaline phosphatase (ALP).

https://doi.org/10.1038/s41561-022-01105-y

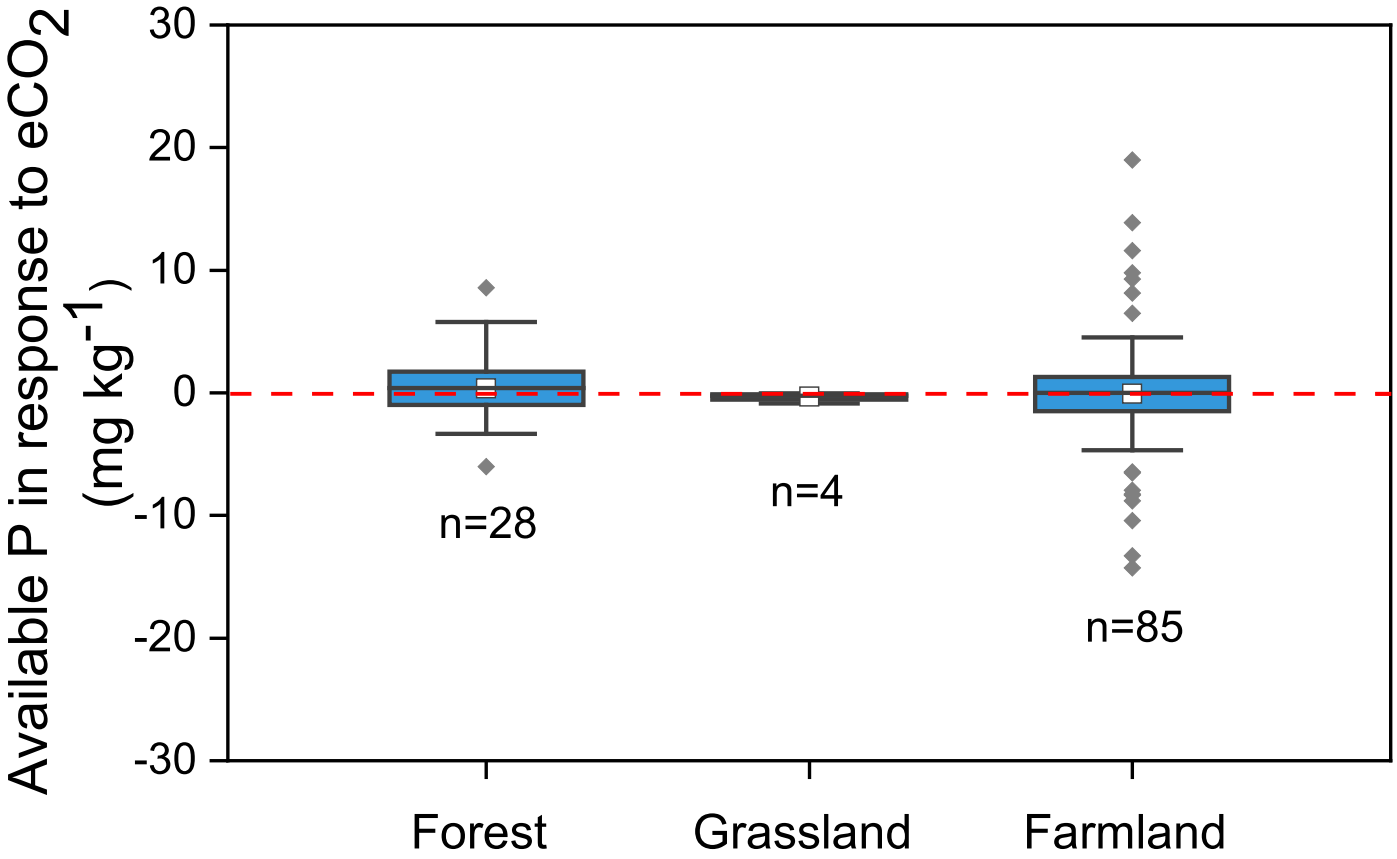

Extended Data Fig. 7 | Soil available P under eCO_2 relative to aCO_2 in different systems based on new data from this study for farmland and the literature. The values indicate the change (eCO_2 - aCO_2) for soil P pool sizes due to eCO_2. Soil available P includes different indices including resin P, $NaHCO_3$-P_i, and Olsen P (shown in Supplementary Table 1). The line and empty square in each box represent the median and mean, respectively. Whiskers mark the 10th and 90th percentiles, and the outliers are shown as dots. The number of experimental outcomes was defined as n.

https://doi.org/10.1038/s41561-022-01105-y

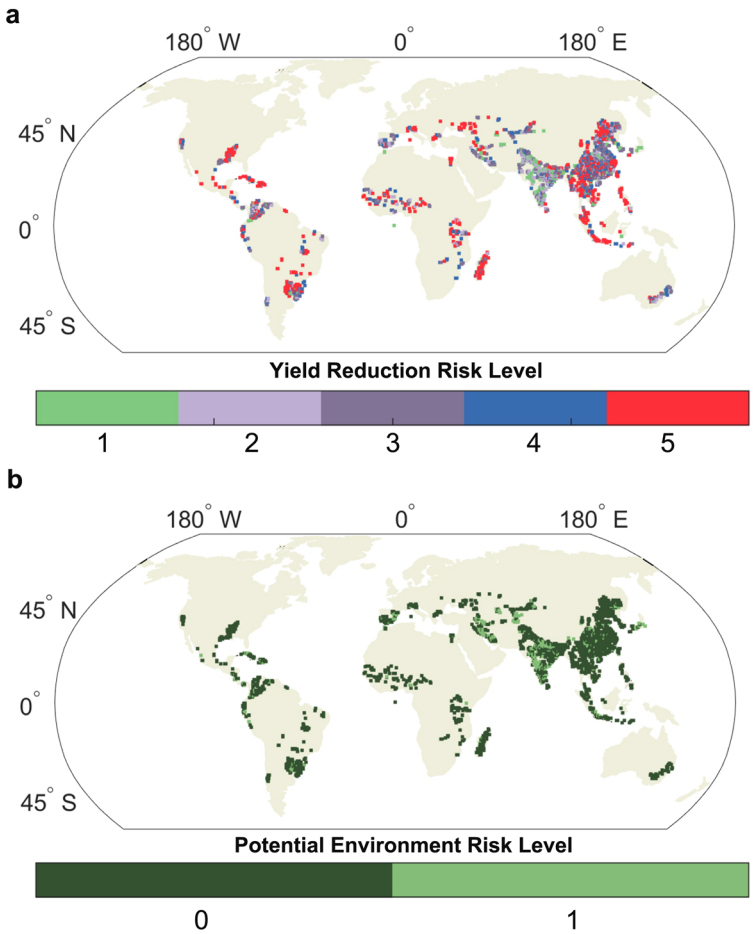

Extended Data Fig. 8 | Global distribution of rice yield reduction and potential P pollution risk. a, Global distribution of yield reduction risk level (1: extremely low, 2: low, 3: medium, 4: high, 5: extremely high; see Methods). **b**, Global distribution of potential P pollution risk level (0: no risk, 1: with potential environment risk). Note the size of the squares does not represent the actual area of rice paddy fields in Panels a and b.

https://doi.org/10.1038/s41561-022-01105-y

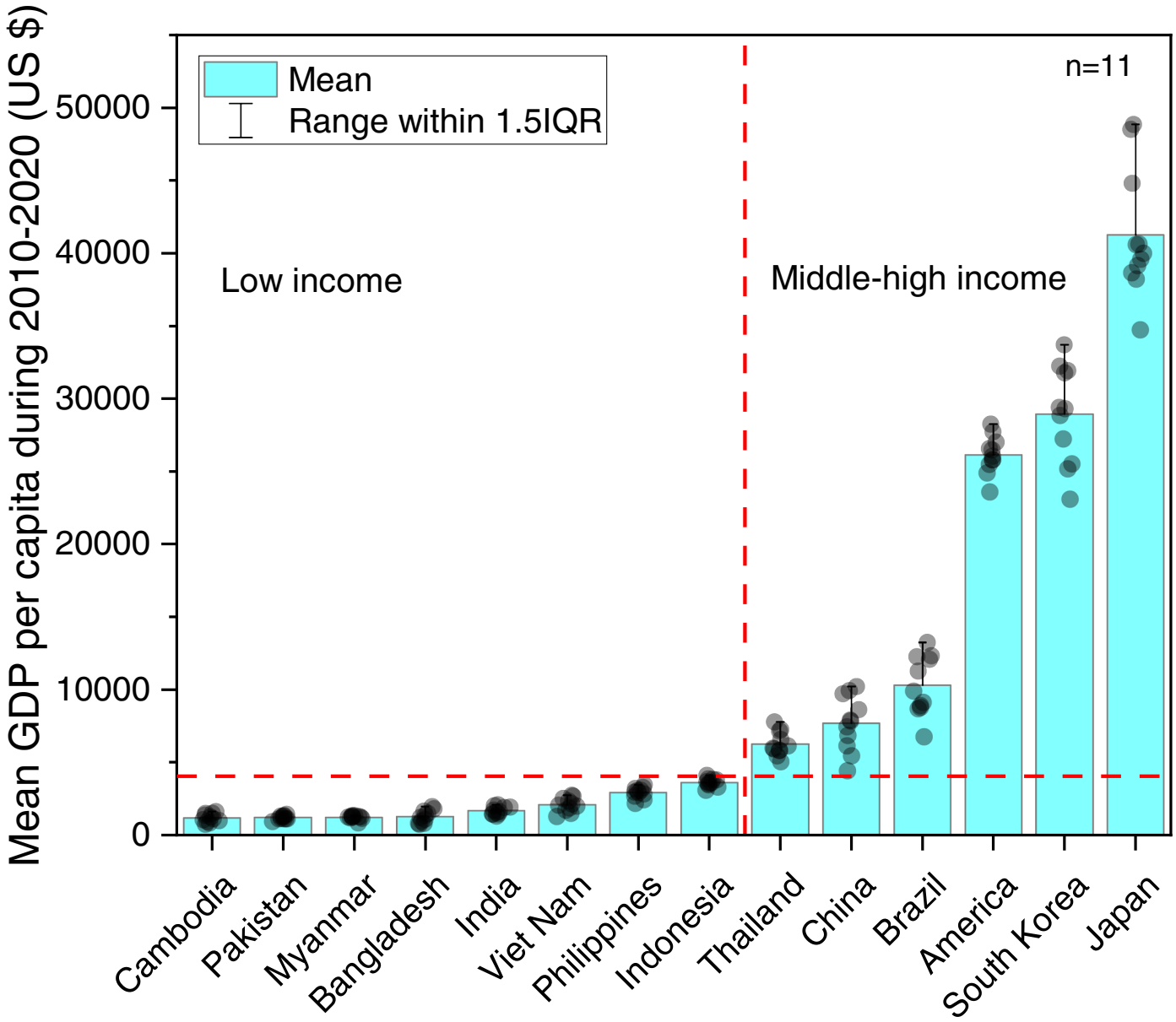

Extended Data Fig. 9 | Bar plot of mean GDP per capita during 2010–2020 for 14 global rice grown countries according to the 2019 World Bank income classifications. The error bar indicates the standard deviation of GDP per capita during 2010–2020, the horizontal red dash line indicates the threshold value for low-income and middle-high income countries, and the vertical red dash line indicates the grouping of low-income and middle-high countries. The IQR indicates the interquartile range.

https://doi.org/10.1038/s41561-022-01105-y

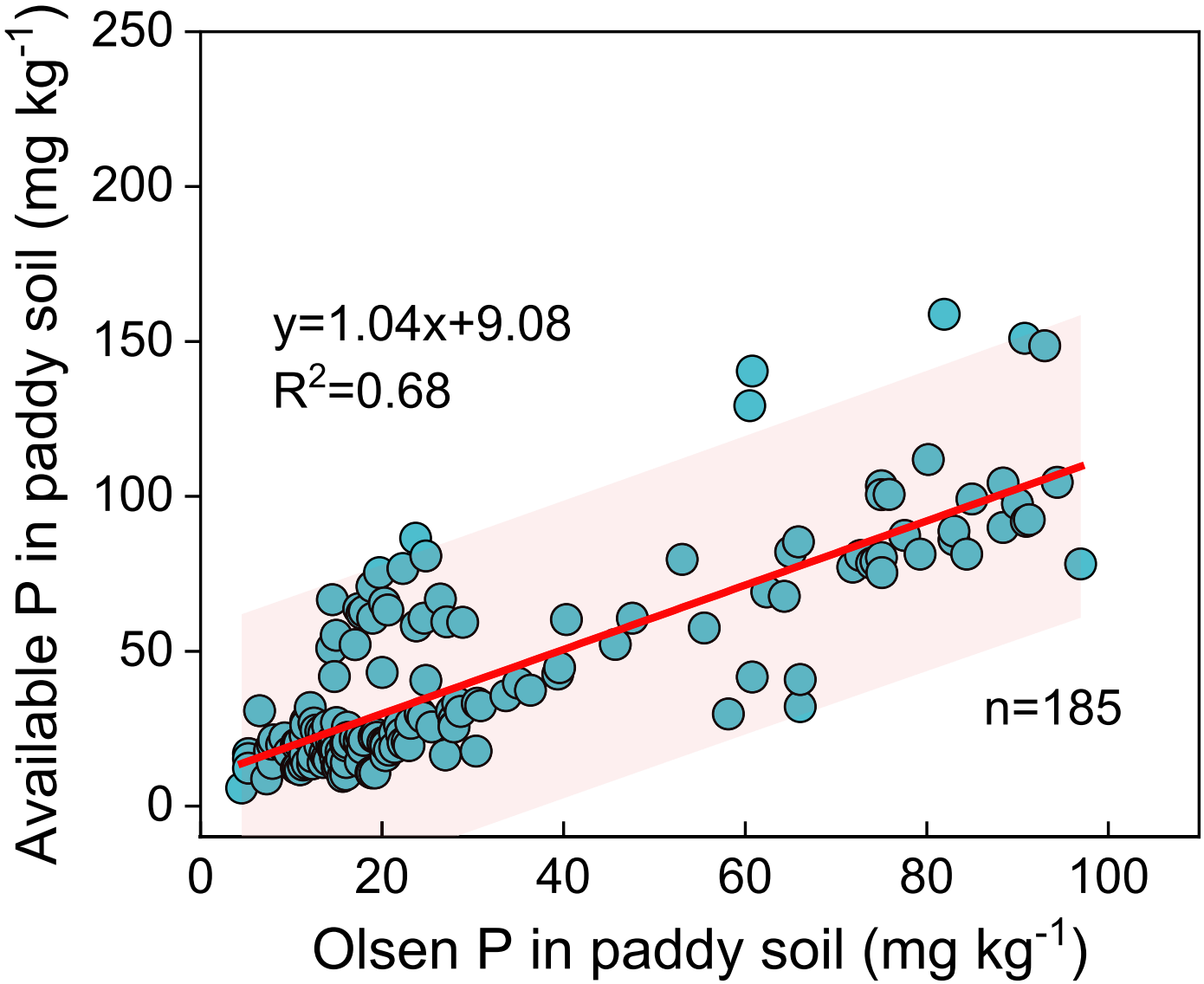

Extended Data Fig. 10 | Relationship between Olsen P and available P in paddy soil. The data are from references[76–81]. The shaded area represents the 95% confidence interval for the fitted line.